Photochemistry and Photobiology, 2007, 83: 782–792

Photobleaching of Dissolved Organic Material from a Tidal Marsh-Estuarine System of the Chesapeake Bay†

Maria Tzortziou*[1], Christopher L. Osburn[2] and Patrick J. Neale[3]

[1]Earth System Science Interdisciplinary Center, University of Maryland, College Park, MD
[2]US Naval Research Laboratory, Washington, DC
[3]Smithsonian Environmental Research Center, Edgewater, MD

Received 4 October 2006; accepted 1 March 2007; DOI: 10.1111/j.1751-1097.2007.00142.x

ABSTRACT

Wetlands and tidal marshes in the Rhode River estuary of the Chesapeake Bay act as important sources of dissolved organic carbon and strongly absorbing dissolved organic matter (DOM) for adjacent estuarine waters. The effects of solar exposure on the photochemical degradation of colored DOM (CDOM) were examined for material derived from different sources (estuarine and freshwater parts of the Rhode River, sub-watershed stream, marshes) in this estuarine ecosystem. Consistent with changes in fluorescence emission, absorption loss upon exposure to different portions of the solar spectrum (*i.e.* different long-pass cut-off filters) occurred across the entire spectrum but the wavelength of maximum photobleaching decreased as the cut-off wavelength of the filter decreased. Our results illustrate that solar exposure can cause either an increase or a decrease in the CDOM absorption spectral slope, S_{CDOM}, depending on the spectral quality of irradiation and, thus, on the parameters (*e.g.* atmospheric composition, concentration of UV-absorbing water constituents) that affect the spectral characteristics of the light to which CDOM is exposed. We derived a simple spectral model for describing the effects of solar exposure on CDOM optical quality. The model accurately, and consistently, predicted the observed dependence of CDOM photobleaching on the spectral quality of solar exposure.

INTRODUCTION

Dissolved organic matter (DOM), a major reservoir of organic carbon in the ocean, plays a central role in many biological and chemical processes in aquatic ecosystems, affecting carbon budgets, nutrient availability and ecosystem productivity (1–3). The colored fraction of DOM, CDOM, is one of the key water constituents determining the underwater light field, affecting ocean color and aquatic photochemistry (4–6). Estuarine and coastal margin ecosystems, such as the Chesapeake Bay and its surrounding wetlands, are complex and dynamic environments of intense DOM cycling in which DOM amount, quality and distribution reflect a balance between inputs and decomposition. In these systems, inputs include seasonal *in situ* production and organic matter of terrestrial and intertidal origin introduced through river run-off, wetland discharges and tidal exchanges (*e.g.* 1,7–9). Despite large inputs, DOM of terrestrial and intertidal origin contributes only a small part of the total DOM pool in the global ocean, suggesting rapid cycling and high mineralization rates of these components within estuaries and coastal marine environments (10,11).

Photochemical and biological degradation processes play critical roles in regulating the residence time, cycling and fate of CDOM and dissolved organic carbon (DOC) in near shore waters (*e.g.* 12,13). Biological degradation is mediated primarily by bacterioplankton that use the labile DOM fraction for growth and respiration. Photochemical alteration of CDOM during solar exposure generates a variety of photoproducts, including reactive oxygen species (14), atmospherically important trace gases, such as CO, CO_2 and COS (*e.g.* 5), and low molecular weight labile carbonyl compounds that are readily available for consumption by microbial communities (3,15). This photochemical–biological coupling is not completely understood and previous studies have shown that photochemistry may form, as well as destroy, biological carbon substrates (*e.g.* 12,16,17). According to Tranvik *et al.* (18) the net outcome of competing stimulatory and inhibitory effects of photochemical processes on the bioavailability of DOM varies across different environments depending on their water chemistry and on the origin and composition of DOM. Although marsh DOC inputs have been shown to contribute significantly to the carbon budget of the coastal zone (*e.g.* 7,10,19), the composition and optical properties of marsh-derived CDOM remain largely uncharacterized. Thus, we know little about the susceptibility of this material to photodegradation, or on the effects of solar exposure on its bacterial availability. One of the main objectives of this study was to provide some information on the optical quality and photoreactivity of the dissolved organic compounds exported from a tidal marsh system of the Chesapeake Bay. Brackish and freshwater tidal marshes cover a large area (about 70 000 ha) along the western and eastern Bay shores, potentially playing an important role in the complex photochemical and biogeochemical processes taking place in the Bay system.

The change in CDOM chemical structure during solar exposure is reflected in changes in its optical properties (*e.g.* 5,20) that provide a first-order measure of the photoreactivity

†This invited paper is part of the Symposium-in-Print: UV Effects in Aquatic and Terrestrial Environments.

*Corresponding author e-mail: martz@snarktoo.gsfc.nasa.gov, mtzortziou@hotmail.com (Maria Tzortziou)

of CDOM in a water body of interest. CDOM absorption spectra, $a_{CDOM}(\lambda)$, are relatively featureless, typically showing an exponential increase with decreasing wavelength in the UV–visible range (4). The absorption spectral slope coefficient, S_{CDOM}, determines the rate of the exponential decline of CDOM absorption with wavelength and has been found to be typically larger for fulvic acids than humic acids, and to decrease with increasing molecular weight and increasing aromaticity (21,22). Dissolved organic compounds fluoresce when excited by light in the UV-blue wavelength region, with larger, highly aromatic molecules typically showing stronger fluorescence at longer wavelengths (*i.e.* longer than 400 nm) and smaller structures with lower aromatic carbon content contributing mostly to short wavelength emission (23–25). Previous studies suggest that photochemical processes, in addition to the bleaching of CDOM absorption and fluorescence magnitude, modify CDOM absorption and fluorescence spectral characteristics. Moran *et al.* (20) found that solar exposure changed the fluorescence spectral properties of terrestrially-derived CDOM, through preferential photobleaching of fluorophores attributed to terrestrially derived humic substances. Photochemical alterations of the CDOM absorption spectral shape (*i.e.* S_{CDOM}) remain obscure, with some studies showing that solar exposure causes an increase in S_{CDOM} (*e.g.* 5,20,26) and others reporting a decrease in S_{CDOM} during photobleaching (*e.g.* 8,27–29). In most of these studies CDOM was exposed to the full spectrum of natural or artificial sunlight.

The spectral characteristics of the light irradiating DOM in near shore waters depend on various parameters such as latitude, season, atmospheric composition (*e.g.* ozone amounts), water constituents (*e.g.* UV-absorbing detritus and inorganic particles) and water depth. Yet, only a few published studies have focused on how the spectral quality of polychromatic solar exposure affects CDOM photobleaching. One approach to derive a quantitative relationship between CDOM photobleaching and solar spectral irradiance is using apparent quantum yield (AQY) spectra determined by a series of irradiations with monochromatic light (30–32). This approach, however, does not capture potential interaction effects between wavelengths that are present simultaneously in natural sunlight (33,34). Another approach for determining AQY spectra for DOM photoproducts makes use of optical cut-off filters that allow exposure to specific portions of the solar spectrum (*e.g.* 29,30,33,35). Using a series of nine optical cut-off filters and spectral weighting functions (*e.g.* 6), Osburn *et al.* (36) demonstrated the spectral dependency of solar UV photobleaching of CDOM from lake waters. In their study, Osburn *et al.* determined photobleaching as the loss of dissolved absorption averaged over the wavelength band of 280–500 nm. Thus, their approach did not provide information on the spectral shifts in the CDOM absorption spectrum after photobleaching. The main focus of our study was to examine how the spectral quality of solar exposure affects the fluorescence and absorption spectral characteristics of CDOM from different sources (freshwater, estuarine-dominated and marsh-exported DOM) in a highly dynamic, marsh-estuarine system, and, subsequently, derive a simple predictive model to describe these changes.

MATERIALS AND METHODS

Study site and sample collection. The Rhode River is a turbid, eutrophic sub-estuary on the western shore of the Chesapeake Bay in Maryland (38.88°N, 76.53°W). The sub-estuary is surrounded by a 2300-ha watershed, with soils high in nitrogen and phosphorus, and an 88-ha intertidal zone, composed of about 32 ha of mudflats and tidal creek channels, 20 ha of high-elevation marshes and about 36 ha of low-elevation marshes (37). Mean depth in the Rhode River is 2 m, with a maximum of nearly 5 m (38). Salinity varies seasonally from 5 to 18 at the mouth, depending mainly on the flow of the Susquehanna River, and from 0 to 14 at the head, depending mainly on local flow of Muddy Creek, the principal freshwater source to the sub-estuary (39). The mean tidal amplitude in the Rhode River is 0.3 m, but changes in water level are additionally affected by weather conditions (40).

Photobleaching experiments were performed on DOM samples collected from four sites in the Rhode River estuary and watershed, in August and September 2004 (Fig. 1, Table 1). Sample 1A was collected from the mouth of the Rhode River to the Chesapeake Bay (estuarine-dominated sample). Samples 6C and 101 (freshwater-dominated samples) were collected, respectively, from upstream Muddy Creek and from a stream draining a 226-ha subwatershed of the Rhode River having a mixed land use (38% forest, 10% row crops, 27% pasture and hay fields, 6% residential and 19% old fields) (41). Sample HM was collected from water draining off of a tidal marsh at ebbing tide. The high-elevation, brackish Kirkpatrick marsh, south of Muddy Creek (Fig. 1), is 0.4–0.6 m above mean low water and is primarily vegetated by *Spartina patens*, *S. cynosuroides, Distichlis spicata*, *Iva frutescens* and *Scirpus olneyi*. Previous studies suggest that the marsh is fully submerged 2% of the time and that the marsh creek drains an area of about 3 ha (42).

Water samples were filtered using 0.22 μm pore-diameter membrane filters to separate the dissolved material. Filtered water was stored in the dark at 4°C for less than 10 days before exposure to natural sunlight. Before optical analysis the samples were warmed to room temperature.

Photobleaching. To examine the effects of solar exposure on CDOM fluorescence and absorption spectral characteristics, DOM was exposed to natural sunlight over a time period of several days using the methods of Osburn *et al.* (36). A series of eight Schott optical long-pass cut-off filters were used to examine how the spectral quality of light irradiating the dissolved material affects CDOM optical quality. Cut-offs (50% T) for the filters were 288, 305, 317, 332, 357, 375, 389 and 395 nm. In total, we used eight optical treatments, a "no filter" (NF) treatment and a dark control (DK), each composed of two

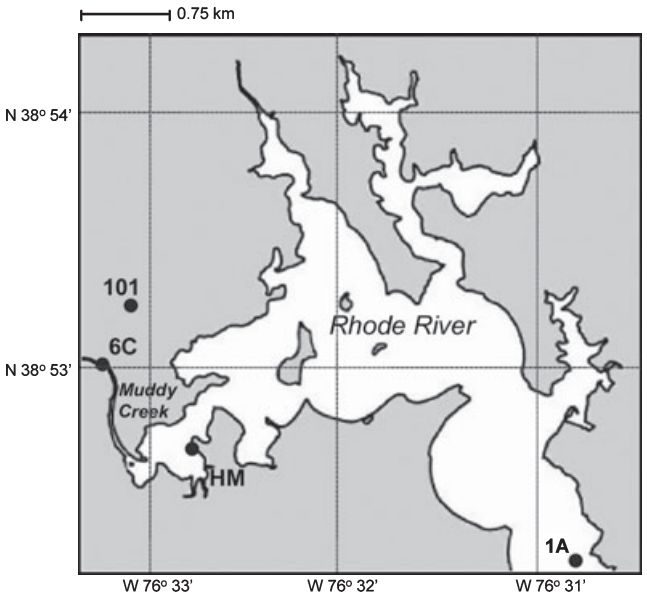

Figure 1. Location of the four sites sampled in the Rhode River sub-estuary.

Sample	Collection date	[DOC] (mg L^{-1})	$SF_{em=365}$	SF_{ratio}	$a_{CDOM}(440)$ (m^{-1})	S_{CDOM} (nm^{-1})	$a^*_{CDOM}(440)$ (m^2 g^{-1})
1A	5 August 2004	5.1	$17{\cdot}10^4$	0.36	0.63	0.0174	0.123
6C	5 August 2004	10.3	$62{\cdot}10^4$	0.41	2.33	0.0168	0.226
101	13 September 2004	6.2	$57{\cdot}10^4$	0.23	1.27	0.0176	0.205
HM	17 September 2004	11.15	$59{\cdot}10^4$	0.63	6.20	0.0148	0.556

Table 1. CDOM fluorescence and absorption properties of samples from the Rhode River and associated watershed before exposure (see Fig. 1 for sample locations).

CDOM = colored dissolved organic matter; DOC = dissolved organic carbon.

replicates. Samples were placed in flanged quartz tubes (15 cm length, 2 cm diameter) and sealed with silicone stoppers wrapped in acid-washed Teflon tape (36) to exclude potential contamination of the sample from compounds shown to leach from silicone (43). The quartz tubes are 99% pure, transmitting well below 280 nm. All exposures occurred on the roof of the Chemistry Building of the US Naval Research Laboratory, Washington, DC. The tubes were placed in black plastic boxes (painted flat black on the inside to minimize reflectance) and were covered with the appropriate filter for exposure at different portions of the solar spectrum. Boxes and tubes were kept at constant temperature during the exposure, floating horizontally at the surface of a tank filled with water.

The samples were exposed to solar radiation for *ca* 3 days (15–18 August for samples 1A, 6C, and 21–23 September for samples 101 and HM) in a water bath to buffer temperature. Solar attenuation by the water bath was negligible. After exposure, samples were stored in the dark at 4°C for less than 1 day until further optical analysis. Measured changes in CDOM optical properties were used to fit a spectral model of solar photobleaching as described in the modeling section.

Dissolved organic carbon. Dissolved organic matter samples were put into cleaned and precombusted (500°C, 5 h) glass vials for dissolved organic carbon analysis. To each vial, a few drops of 85% H_3PO_4 was added to decrease the sample pH to <3, converting all dissolved inorganic carbon (DIC) to CO_2, which was removed by sparging the sample for 10 min with ultrahigh purity He. After removal of DIC, samples were placed in the autosampler of an OI Analytical 1010 TOC Analyzer (College Station, TX) and DOC was measured by heated persulfate oxidation. Two milliliters of sample was injected into the reaction vessel and 5 mL of 200 mg L^{-1} persulfate reagent was added. The sample plus reagent was heated to 98°C for 6 min, converting DOC to CO_2. The CO_2 was purged from the sample with UHP He and swept past a nondispersive infrared detector. Solutions of potassium hydrogen phthalate standard were used to create a calibration curve over the range of 0–833 μmol C L^{-1}. Following the recommendations of McKenna and Doering (44), enough persulfate was added to the sample so that any halogens present would be oxidized along with DOC. Multiple MilliQ water blanks were run until background counts were low and steady before proceeding with sample analysis.

Absorption measurements. Measurements of CDOM absorption were performed using a CARY-IV dual beam spectrophotometer. Due to the high optical thickness of the samples, absorbance measurements were performed using 1 cm pathlength, acid-cleaned, quartz cuvettes. Measurements were baseline corrected using MilliQ water, running a new blank before each sample. Duplicate measurements were performed for each sample. Measurements covered the spectral range from 290 to 750 nm (1 nm bandwidth and interval). CDOM absorption coefficients were estimated from measured optical densities (OD) after multiplying by 2.303 and dividing by the pathlength (0.01 m for a 1 cm cuvette):

$$a_{CDOM}(\lambda) = 2.303\frac{OD}{l_g} = 2.303 \cdot \frac{OD}{0.01}\,(m^{-1}) \qquad (1)$$

Relative absorption change during exposure was calculated as the decrease in absorption (Δa) divided by initial a.

As absorption by CDOM decreases with increasing wavelength in an exponential fashion, the exponential slope, S_{CDOM}, was estimated after applying nonlinear exponential regression to $a_{CDOM}(\lambda)$ values measured in the complete spectral range of the measurements 290–750 nm. R^2 values of the nonlinear exponential fits were in almost all of the cases larger than 0.99. Whereas variability in CDOM absorption reflects changes in both CDOM amount and chemical structure, variability in the mass-specific CDOM absorption is related to variability in CDOM composition. Although not all of DOC is colored, CDOM absorption values at 440 nm were normalized to DOC concentration, $a^*_{CDOM}(\lambda) = a_{CDOM}(440)/[DOC]$, as a measure of CDOM absorption per unit organic carbon in the DOM sample.

Fluorescence measurements. Measurements of CDOM fluorescence were made on a SPEX Fluoromax-3 spectrofluorometer. The fluorescence emission measured by the signal-detector, S_c, was referenced to the signal measured by the reference-detector, R_c, in order to monitor and correct for the wavelength response of the Xenon lamp and excitation monochromator as well as for fluctuations in the lamp power supply, according to the manufacturer's protocol. Emission and excitation correction-factor files were applied according to the manufacturer's instructions to correct for the wavelength dependencies of the optical components of each monochromator and the detectors themselves. Fluorescence spectra were corrected for absorption within the sample (inner-filter effect) according to McKnight *et al*. (25) and using the CDOM absorption spectra measured spectrophotometrically. Bandwidths were set to 5 nm for both excitation and emission. A spectrum of MilliQ water was subtracted as a blank to correct for Raman effects.

The synchronous fluorescence (SF) technique was used as a tool for investigating variability in composition and optical properties of CDOM in this marsh-estuarine system. An SF spectrum is a subset of the excitation–emission matrix in which excitation and emission are at a constant wavelength offset ($\delta\lambda = \lambda_{em} - \lambda_{exc}$) (23,45). Long wavelength features in SF spectra are typically associated with the presence of high molecular weight CDOM of terrestrial origin (24,36,46). A wavelength offset of $\delta\lambda = 14$ nm was used in our SF measurements (λ_{exc} in the range 330–600 nm, 1 nm resolution) based on previous results showing that this wavelength offset is optimal for resolving differences in CDOM between sources (24). This wavelength offset is also a good compromise between more structural features and lower signal to noise ratios in the SF spectra.

Spectral irradiance. Irradiance in the range 290–330 nm was measured with a narrow band, multi-filter radiometer, the SR18 (designed, fabricated and calibrated by the Solar Photobiology Laboratory of the Smithsonian Environmental Research Center). Full description of the instrument characteristics is given by Neale *et al*. (47). Briefly, the instrument consists of a cosine-corrected diffuser, interference filters that are rotated through the light path on a filter wheel and a solar-blind photo-multiplier tube. Incident solar UV-B spectrum is defined with 18 filters with nominal 2 nm full width at half-maximum (FWHM) bandwidths, spaced at 2 nm intervals from 290 to 324 nm. A 19th channel measures the far UV-A at 330 nm with a 10 nm FWHM bandwidth interference filter. The instrument was located adjacent to the exposure site and spectra were acquired at 4 s intervals and recorded as 12 min averages. These spectra were extended over the UV and PAR range (290–700 nm) using a radiative transfer model (System for Transfer of Atmospheric Radiation or STAR) using the procedure described by Neale *et al*. (47). Spectra of cumulative incident radiant energy over the exposure period were multiplied by the spectral transmission of each treatment. Absorbed energy ($H_a(\lambda)$, J m^{-2} nm^{-1}) for each treatment was calculated using the procedure of Osburn *et al*. (36).

Spectral photobleaching model. Measured changes in CDOM optical properties were used to estimate parameters of a spectral model of photobleaching. We modeled the relative change in CDOM absorption at wavelength λ_o, $\Delta a/a$ (λ_o), according to:

$$\frac{\Delta a}{a}(jj,\lambda_o) = \int_{200\,\mathrm{nm}}^{700\,\mathrm{nm}} H_a(jj,\lambda)\cdot W(\lambda)\cdot WSF(\lambda,\lambda_o)\cdot d\lambda + c_2 \qquad (2)$$

where λ_o is the wavelength where we measure the absorption loss, *jj* is the cut-off filter (irradiation treatment), integration is over the spectral range 200 to 700 nm, $H_a(jj, \lambda)$ is the absorbed solar exposure (J m^{-2} nm^{-1}) at wavelength λ for the cut-off filter *jj*, $W(\lambda)$ is the spectral efficiency for photobleaching (relative absorption change per [J m^{-2}]) modeled as $W(\lambda) = \exp(m_o + m_1\cdot\lambda)$, $WSF(\lambda, \lambda_o)$ (nondimensional) is the wavelength spread function (assumed here to be Gaussian), $\mathrm{WSF}(\lambda,\lambda_o) = \exp(-\frac{(\lambda-(\lambda_o+c_1))^2}{\mathrm{spread}^2})$, spread is related to the FWHM bandwidth for the Gaussian spread function ($\mathrm{FWHM} = 2\cdot\sqrt{\ln 2}\cdot\mathrm{spread}$), and c_1 (nm), c_2 (nondimensional) are constants for a wavelength offset in the Gaussian function and nonspectral photobleaching, respectively. While the nonspectral bleaching component is represented by a constant (c_2) in our analysis, we expect that it actually must depend on parameters such as total amount of irradiation and CDOM photo-reactivity. As will be shown later, a constant gives a good fit for the data presented here due to the small size of the component (see Results section) and similarity in total irradiance between treatments. Solar simulator exposures (currently underway) with a larger range of irradiance will hopefully provide sufficient data to formulate a more general representation in the future. The choice of functional form of the spread function, which was guided by previous results on the multiple wavelength effects of monochromatic exposure (32), is discussed in more detail in the Results and Discussion sections.

Parameters were estimated using nonlinear regression of predicted *vs* observed $\Delta a/a$ (jj, λ_o), minimizing RMS error over the spectral range of 290–450 nm for each sample. 95% confidence intervals were estimated from the asymptotic variance–covariances of final parameter estimates, using the number of treatments—number of parameters as a conservative estimate of the degrees of freedom of *t*. Calculations were performed in MATLAB using the nlinfit and nlparci functions.

RESULTS

DOC concentrations

Concentrations of DOC before exposure to solar radiation were 5.1 and 10.3 mg L^{-1}, respectively, at the estuarine (station 1A) and freshwater (station 6C) parts of the Rhode River in August (Table 1). Freshwater sample 101, collected from the subwatershed stream in September, had initial [DOC] of 6.2 mg L^{-1}, while water draining off of the Kirkpatrick marshes 4 days later was almost two-fold higher in DOC, with [DOC] = 11.15 mg L^{-1}.

Solar exposure effects on CDOM fluorescence

Initial (before exposure) fluorescence characteristics were considerably different among the four collected CDOM samples (Fig. 2, dark control), reflecting the differences in concentration and composition of CDOM in the Rhode River estuarine environment. Sample 1A, collected from the estuarine-dominated waters at the mouth of the Rhode River to the Chesapeake Bay, had the lowest SF (fluorescence was also lower relative to the other samples over the whole surface of excitation–emission matrices, data not shown). SF at emission 365 nm was of similar magnitude in the freshwater and marsh-derived DOM samples (6C, 101 and HM; Table 1), and more than three times stronger compared with 1A. However, CDOM exported from the Kirkpatrick marshes (sample HM) had much stronger SF signal at wavelengths longer than 400 nm, which is typical of terrigenous, plant- or soil-derived CDOM (*e.g.* 24). The fluorescence ratio $\mathrm{SF}_{\mathrm{em}=490}/\mathrm{SF}_{\mathrm{em}=365}$, a measure of the importance of longer wavelengths in the SF spectrum, was 0.63 for the CDOM draining off of the marshes at ebbing tide, relative to 0.36, 0.41 and 0.23 for samples 1A, 6C and 101, respectively (Table 1).

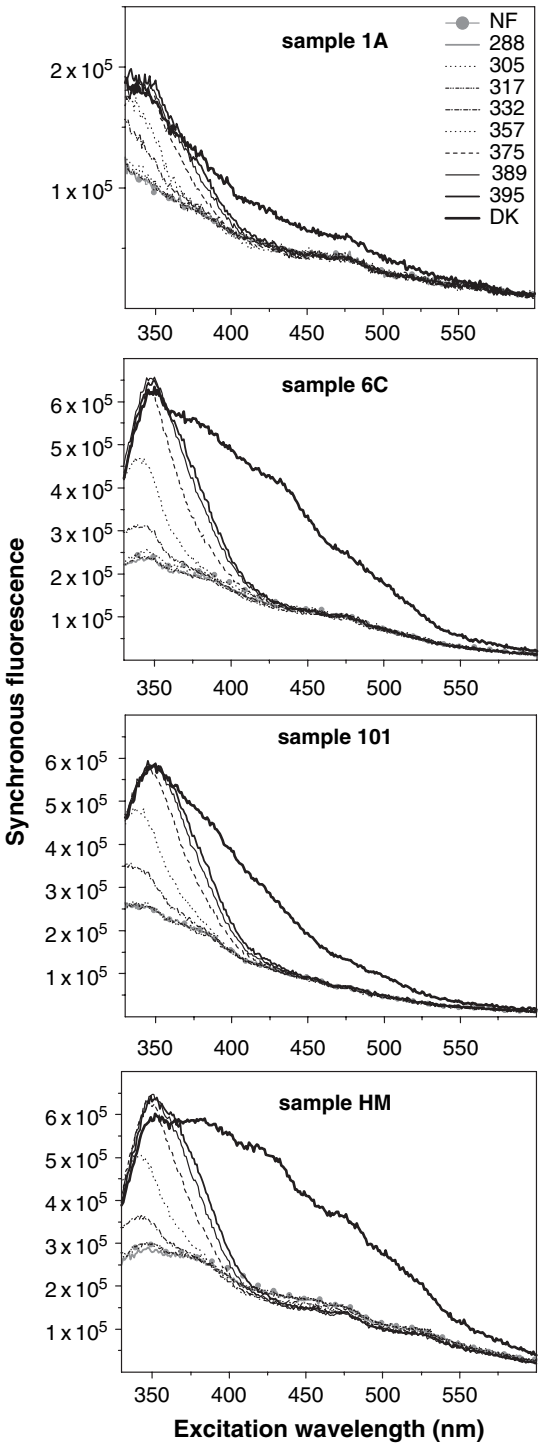

Figure 2. Change in CDOM synchronous fluorescence ($\delta\lambda$ = 14 nm) after solar exposure, for the eight optical treatments, the "no filter" treatment (NF, *cf.* exposure to the full solar spectrum), and the dark control (DK). Results are shown for all samples from the Rhode River (one of the two replicates, almost identical results for the other).

Solar exposure (*ca* 3 days, see Materials and Methods) resulted in a substantial loss of CDOM fluorescence. For exposure to the full spectral range of natural sunlight (NF treatment, solid circles in Fig. 2), the fraction of SF loss, averaged over the measured spectral range (330–600 nm), to the initial SF, averaged over the same spectral range, was 0.34 for sample 1A and more than 50% (0.61, 0.55 and 0.54, respectively) for samples 6C, 101 and HM. The fluorescence ratio $SF_{em=490}/SF_{em=365}$ after exposure was 0.42, 0.42, 0.27 and 0.53 for samples 1A, 6C, 101 and HM, respectively.

Use of different cut-off filters showed that fluorescence fading occurred in different regions of the spectrum depending on the spectral characteristics of the light irradiating CDOM (Fig. 2). For a cut-off filter of 395 nm (50% filter transmission at 395 nm) most of the fluorescence loss was observed at $\lambda > 390$ nm. As the cut-off moved to shorter wavelengths, additional loss of fluorescence was observed at the shorter UV wavelengths.

Effects of solar exposure on CDOM absorption

Similar to the fluorescence analysis, large differences were found in the initial absorption characteristics among the four CDOM samples collected from the Rhode River (Table 1). Sample 1A had the lowest absorption, $a_{CDOM,}$ and the lowest DOC-specific absorption, a^*_{CDOM}, across the spectrum (values are shown only at 440 nm in Table 1). Marsh-exported CDOM was the most strongly absorbing among all samples ($a^*_{CDOM}(440)$ more than twice as large as that of the freshwater samples 6C and 101) and its absorption spectral slope of 0.0148 nm^{-1} was lower than that of the other samples (S_{CDOM} between 0.0168 and 0.0176 nm^{-1} for 1A, 6C and 101).

Solar exposure of CDOM considerably reduced absorption in all samples. For exposure to the full spectrum of natural sunlight (NF treatment), the loss of absorption averaged over the range 290–500 nm

$$\Delta a_{avg} = \frac{\sum_{\lambda=290}^{500} a_{CDOM}(\lambda)_{init} - a_{CDOM}(\lambda)_{treat}}{210} \qquad (3)$$

(similar to the quantity PBavg estimated by Osburn *et al*., 36), was 0.38, 2.49, 1.29 and 3.92 m^{-1} for samples 1A, 6C, 101 and HM, respectively. These absorption losses correspond to fractional absorption losses of 18%, 29%, 27% and 22% for the four samples, respectively. CDOM photoreactivity, estimated as the ratio of Δa_{avg} to the total energy absorbed by the exposed sample (expressed as m $J^{-1} \times 10^{-6}$ cf. Osburn *et al.,* 36) was 2.1, 3.9, 3.4 and 2.8 for samples 1A, 6C, 101 and HM, respectively.

The cut-off filter experiments showed a progressive bleaching of CDOM absorption as treatments included more UV radiation (Δa_{avg} is shown for all treatments for sample HM in Fig. 3). Moreover, consistent with the fluorescence measurements, the greatest loss of absorption occurred in different regions of the spectrum depending on the spectral characteristics of the light irradiating CDOM (Fig. 4). For a cut-off filter of 395 nm, absorption fading was more pronounced at wavelengths longer than ~390 nm. The relatively stronger loss of absorption at the longer UV wavelengths resulted in an increase in S_{CDOM} compared to the dark treatment (DK) (Fig. 5). As the cut-off moved to shorter wavelengths (*e.g.* 50% transmission wavelength of cut-off filter shorter than 332 nm), additional loss of absorption was observed at the shorter UV wavelengths, with a subsequent decrease in S_{CDOM}. This spectral dependence of CDOM photobleaching, and the resulting change in S_{CDOM}, was consistent among all CDOM samples, despite the large differences in their initial absorption characteristics.

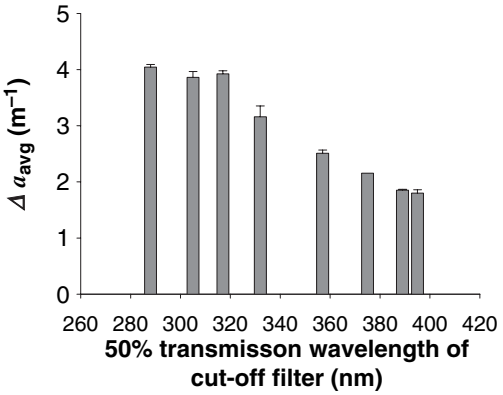

Figure 3. Photobleaching in the HM sample (CDOM exported from the Kirkpatrick tidal marsh) *vs* the 50% transmission wavelength measured for each cut-off filter treatment. Error bars show half range for two replicates. *P*-value for one-way ANOVA was less than 0.0001.

Spectral model of photobleaching

Measured changes in CDOM optical properties were used to fit the parameters for a spectral model of UV photobleaching. We modeled the relative change in CDOM absorption at wavelength λ_o, for treatment *jj*, $\Delta a/a$ (λ_o, *jj*), according to (Eq. 2). Model runs were qualitatively very similar among the different samples, and thus detailed results are shown here only for CDOM derived from the watershed stream (sample 101; Fig. 6). Parameter values obtained for all runs are shown in Table 2. Model runs were not performed for the estuarine-dominated sample 1A because of the relatively small a_{CDOM} and Δa values measured for this sample and the large noise in the estimated $\Delta a/a$.

For the stream-derived CDOM, the maximum in measured $\Delta a/a$ varied from 20% to 33% between treatments (Fig. 6a,b). Of that, nonspectral bleaching (parameter c_2) was estimated to be about a 5% change in absorption, so spectral bleaching accounted for approximately 75–85% of photobleaching at the wavelength of maximum change. The estimated weighting function for bleaching efficiency of absorbed energy ($W(\lambda)$, m^2 J^{-1}) varied only slightly with wavelength, *i.e.* the spectral slope parameter, m_1, was close to zero. Indeed, m_1 was slightly positive for all samples, though not significantly for sample 6C (Table 2). Photobleaching weights at 300 (UV-B photoreactivity) and 380 nm (UV-A photoreactivity) were $1.66 \cdot 10^{-6}$ and $2.01 \cdot 10^{-6}$ m^2 J^{-1}, respectively, for stream-derived CDOM.

The spread function had an estimated FWHM of ~50 nm. However, the maximum photobleaching effect was predicted to be significantly blue-shifted (by ~29 nm) with respect to the wavelength of exposure (parameter c_1). The model fit implies that spectral exposures photobleached mostly in a blue-shifted band extending from the wavelength of exposure (λ_{irr}) to λ_{irr}-54 nm (= 29 + 50/2 nm). This blue-shift in the photobleaching effect relative to the wavelength of exposure also has been observed in monochromatic exposures of humic acids (30,32).

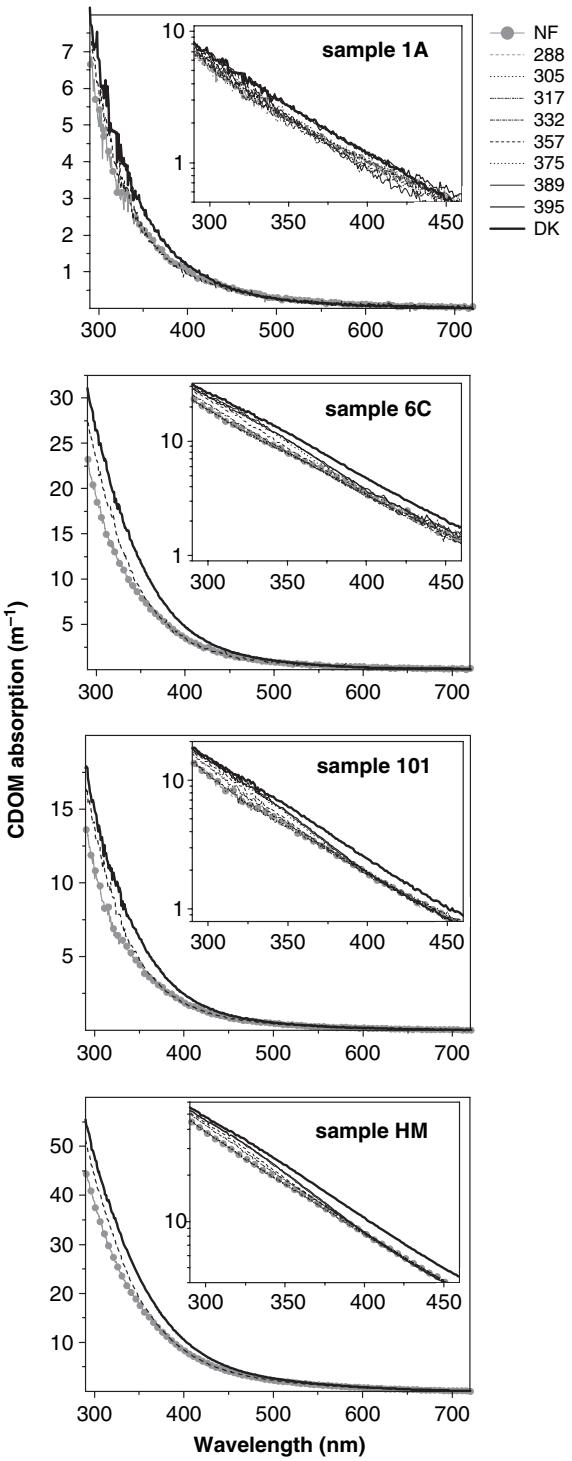

Figure 4. Change in CDOM absorption spectra (290–720 nm) for samples 1A, 6C, 101 and HM (one of the two replicates shown here, almost identical results for the other), for exposure to the full solar spectrum (NF; line with solid circles), exposure under the 357 nm cut-off filter treatment (dashed line) and the dark control (DK; thick solid line). The change in a_{CDOM} for all (eight) optical treatments is shown in log-scale at the inset figures (290–460 nm).

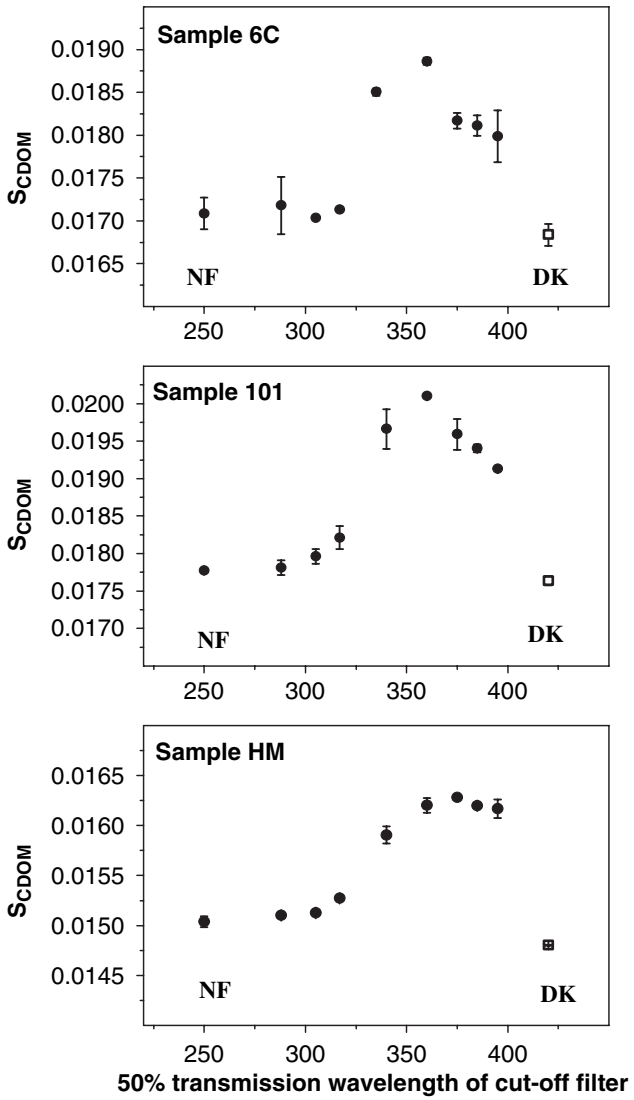

Figure 5. Change in S_{CDOM} for samples 6C, 101 and HM after solar exposure for the eight optical treatments and the "no filter" treatment (NF) (solid circles). The dark control (DK) is also shown (open squares). S_{CDOM} (nm^{-1}) was estimated after applying nonlinear regression to a_{CDOM} values measured in the 290–750 nm range. Error bars show half range for two replicates.

The model successfully predicted that the wavelength of maximum $\Delta a/a$ decreases as the cut-off wavelength of the filter decreases (Fig. 6a,b). Based on the predicted $\Delta a/a$, we calculated the predicted final absorption curves for each treatment and compared S_{CDOM} over the modeled range (290–450 nm) for both observed and predicted absorption spectra. Consistent with our measurements, the model predicted a differential loss of absorption that results, initially, in an increase in S_{CDOM} compared to the dark treatment and a subsequent decrease in S_{CDOM} as the wavelength of irradiation decreases (Fig. 6c,d). The wavelength offset parameter (c_1) was a critical feature of the model in relation to the predicted S_{CDOM}. Without this offset, $\Delta a/a$ in the short UV-B wavelengths was much smaller (and, thus, S_{CDOM} higher) than observed for the shorter (50% transmission < 357 nm) wavelength cut-offs (results not shown). Overall, predicted S_{CDOM} values were in very good agreement with measurements (Fig. 7). Linear least squares regression of model predicted on measured S_{CDOM} showed strong correlation ($R^2 = 0.97$, $P < 0.0001$) with a slope close to 1 and a relatively small intercept ($Y = 0.93X + 0.001$). The observed decrease in S_{CDOM} is still slightly greater than

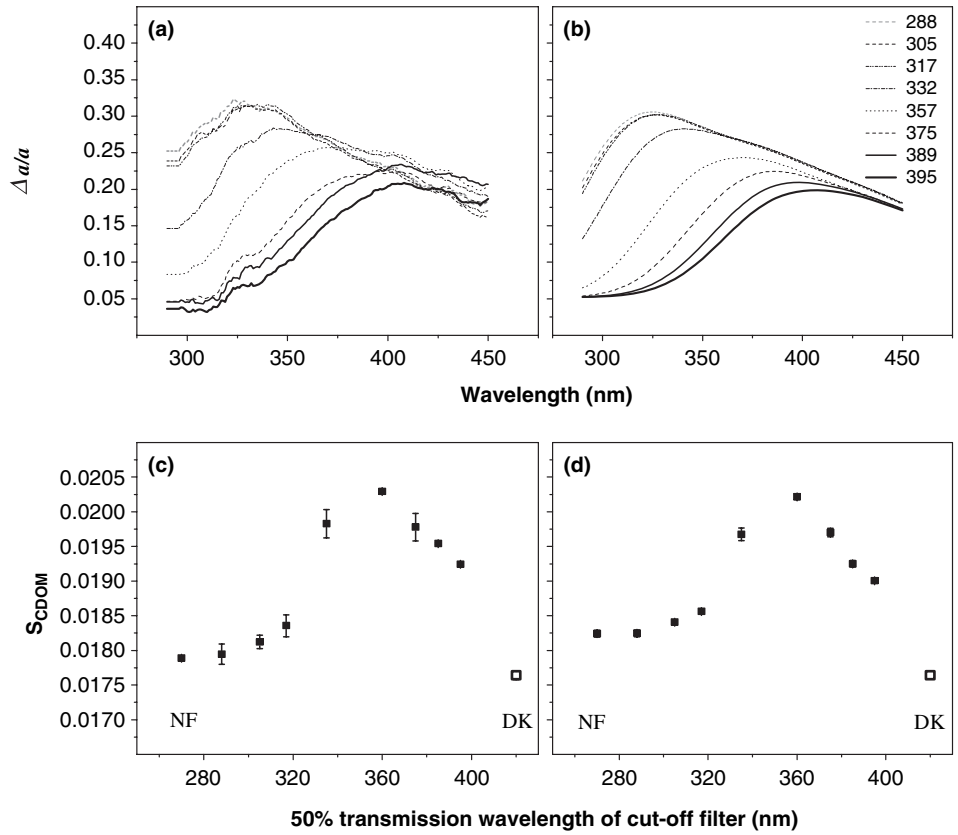

Figure 6. (a) Measured $\Delta a/a$ for the sub-watershed stream-derived CDOM (station 101) and (b) $\Delta a/a$ as predicted by the model for different optical treatments. (c) Measured and (d) model predicted change in S_{CDOM}, for exposures using different cut-off filters, and the "no filter" (NF) treatment. The dark control (DK) is also shown. As $\Delta a/a$ is estimated in the 290–450 nm wavelength range, the S_{CDOM} values shown here were derived after applying nonlinear regression to a_{CDOM} values in the range 290–450 nm. Error bars show half range for two replicates.

Table 2. Parameter estimates obtained by fitting the spectral model of photobleaching (Eq. 2) for CDOM that is marsh-exported (HM), watershed-derived (101), and from the freshwater part of the Rhode River (6C). The half-range of the 95% confidence interval of the estimate is shown in parenthesis.

	HM	101	6C
m_o (n.d.)	−15.45 (0.08)	−14.03 (0.08)	−14.06 (0.2)
m_1 (nm^{-1})	0.0018 (0.0002)	0.0024 (0.0002)	0.0001 (0.0005)
spread (nm)	31.2 (1.6)	29.4 (1.5)	55.5 (3.4)
c_2 (n.d.)	0.057 (0.003)	0.051 (0.004)	0.047 (0.01)
c_1 (nm)	28.6 (0.9)	28.6 (0.9)	26.6 (2.4)

predicted for the shortest cut-offs (*e.g.* 288 nm and NF), because of a small underestimation of $\Delta a/a$ near 290 nm for these treatments (Fig. 6a,b). The estimate can be improved by adding a second band of spectral photobleaching close to 300 nm (as observed by Del Vecchio and Blough, 32), but the improvement is too small to justify the additional two parameters (height and bandwidth of secondary peak) in the model (results not shown).

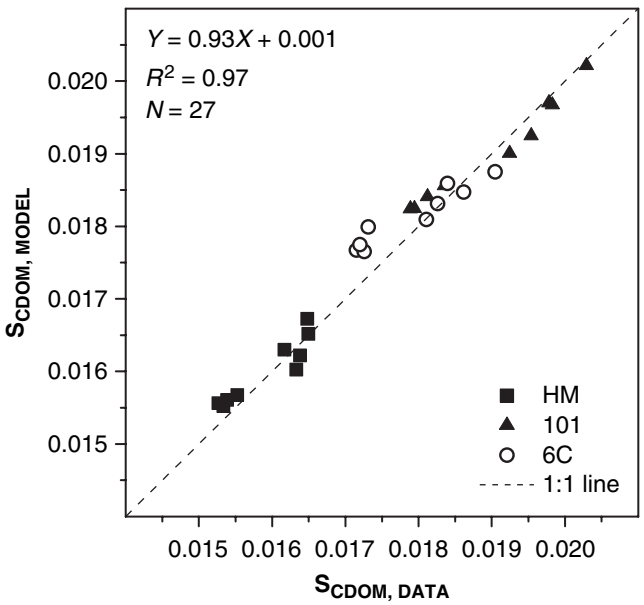

Figure 7. Measured (x-axis) and model predicted (y-axis) S_{CDOM} values for solar exposure using different cut-off filters and the "no filter" treatment (NF), for the marsh-exported CDOM (HM, solid squares), the sub-watershed stream CDOM (101, solid triangles) and CDOM from the freshwater part of the Rhode River (6C, open circles). The 1:1 relationship is shown as dashed line for comparison.

DISCUSSION

Solar exposure changes the composition of terrestrially-derived and biologically refractory DOM in estuarine and

coastal waters through direct photochemical mineralization, secondary photochemical reactions and formation of biologically labile photoproducts (*e.g.* 12,20,48,49). Because the effects of solar exposure on DOC mineralization, CDOM optical quality and DOM bioavailability depend partly on the source and composition of DOM, the DOM samples used in our photobleaching experiments were collected from different sites in the Rhode River, representative of the major sources of DOM in this estuarine ecosystem (*i.e.* freshwater and estuarine parts of the river, watershed stream-derived and marsh-exported DOM). As a result, these samples were considerably different in composition and DOC concentration and, thus, had considerably different initial optical characteristics. Both freshwater samples 6C and 101 had higher DOC concentrations, as well as stronger DOC-specific absorption and fluorescence, relative to the estuarine-dominated sample 1A, consistent with a higher percentage of terrestrially-derived, strongly absorbing and strongly fluorescent, humic-like organic compounds. The most optically distinctive, and, thus, probably also chemically distinctive, DOM sample was collected from the tidal marsh creek. In addition to being particularly enriched in DOC, DOM in the water draining off of the Kirkpatrick marsh had the highest DOC-specific absorption, the lowest S_{CDOM} and relatively stronger fluorescence at wavelengths longer than 400 nm. Each one of these optical characteristics is indicative of humic substances of relatively high aromatic carbon content and high molecular weight (*e.g.* 21,22,24). Additional measurements by our group confirm these results (M. Tzortziou, P.J. Neale, C.L. Osburn, P.J. Megonigal, N. Maie and R. Jaffe, unpublished).

Considerable loss of CDOM was measured in all samples upon exposure to the full spectrum of natural sunlight, with fluorescence loss being more extensive than absorbance fading in agreement with studies by Miller *et al.* (33). However, compared with the samples collected from the Rhode River watershed edge (marsh, watershed stream and upstream Muddy Creek), estuarine-dominated DOM was more resistant to photobleaching. Previous exposure of CDOM to solar radiation during transport from the head to the mouth of the estuary could partly explain such a decrease in the photoreactivity of CDOM along the estuarine gradient (36,50–52). According to Vahatalo and Wetzel (48), the rates of photochemical reactions are expected to be the highest at interfaces where unexposed CDOM enters from shaded environments to regions where it is exposed to unshaded solar radiation. Interfaces like the high-elevation Kirkpatrick marsh, where large concentrations of colored DOC are exported to the adjacent estuarine waters, would, thus, be expected to be hotspots of intense DOM photochemical transformation and cycling.

Use of long-pass cut-off filters allowed us to examine the spectral dependence of CDOM photobleaching. This method was first applied to the calculation of spectral weighting functions for CDOM photobleaching by Osburn *et al.* (36). In agreement with the results presented in that study, we found that absorption loss in CDOM samples from the Rhode River marsh-estuarine system was progressive in treatments that included more UV radiation, with the greatest increment in average absorption loss occurring between filters that included successively more UV-A radiation. However, we note that at least 40% of integrated absorption loss occurred because of the "blue-light" region of the solar spectrum (Fig. 3). Based on the SF loss measured at $\lambda > 400$ nm, that 40% could be due to very reactive humic compounds abundant in the marsh samples.

Moreover, use of the cut-off filters in our study revealed how the spectral quality of solar exposure affects the CDOM absorption and fluorescence spectral shape. Interestingly, the dependence of the changes in SF spectra and S_{CDOM} on the spectral quality of solar exposure was very consistent among all samples, despite differences in their initial DOC concentration, optical characteristics and photoreactivity. In all cases, CDOM bleaching (both absorption and fluorescence loss) was more pronounced at and above the cut-off wavelength of the long-pass filter. However, residual absorption losses were observed throughout the measured spectral range (*e.g.* considerable loss of absorption at 300 nm, even under the 395 cut-off filter treatment, Fig. 6a). Our results are consistent with previous laboratory experiments using monochromatic (laser) sources (30), showing that such exposures result in losses of absorption across the entire spectrum, with the largest loss at or just below the wavelength of irradiation, λ_{irr} (direct photobleaching) and additional "uniform" loss of absorption outside the primary bleaching band (*i.e.* away from the λ_{irr}).

The observed preferential loss of absorption at the wavelengths of irradiation affects the absorption spectral slope, S_{CDOM}, in such a way that environmental exposures may result in either an increase or a decrease in S_{CDOM}, depending on the irradiation spectral characteristics and previous light exposure. As a result, atmospheric composition (*e.g.* ozone and aerosol amounts) and concentration of UV-absorbing water constituents also determine changes in CDOM absorption spectral slope through their effect on the spectral characteristics of the light to which CDOM is exposed.

In previous studies that examined the effects of photobleaching on S_{CDOM}, some reported an increase in S_{CDOM} upon light exposure (*e.g.* 5,20,26,29) while others reported a decrease in S_{CDOM} (*e.g.* 8,27,28). Although this inconsistency could be partly due to the use of different methods in calculating S_{CDOM} (*e.g.* nonlinear fitting of a_{CDOM} *vs* linear fitting of $\log[a_{CDOM}]$, different absorption spectral regions covered), it could also be due to differences in the spectral characteristics of the light to which CDOM was exposed in the different photobleaching experiments. Del Vecchio and Blough (30) measured S_{CDOM} changes during photobleaching of CDOM from the upper Delaware Bay and the mouth of the Chesapeake Bay using polychromatic irradiation and three cut-off filters ($\lambda_{irr} > 320$, > 360 and > 400 nm). They concluded that the observed preferential loss of absorption in the spectral region passed by the cut-off filter resulted in an increase in S_{CDOM} during photobleaching. However, the measured increase in S_{CDOM} under the 360 nm cut-off filter treatment was larger (for same irradiation time) than the increase in S_{CDOM} under exposure to shorter UV light with the 320 nm cut-off filter treatment (their table 2). These results are in agreement with the S_{CDOM} changes observed in our study under the 395, 357 and 332 nm cut-off filter treatments (Fig. 5). CDOM exposure to even shorter UV light using lower cut-off filters resulted in more extensive absorption loss at shorter UV wavelengths, with a subsequent decrease in S_{CDOM}. As a result, S_{CDOM} values for the 288 nm cut-off filter and the NF treatment were very close to the initial S_{CDOM} before photobleaching.

Although this dependence of S_{CDOM} change on the spectral quality of solar exposure has not been previously described (to our knowledge) for natural waters, a similar pattern of change in S_{CDOM} can be found in results reported for CDOM in coastal waters (33). As part of their study on the photochemical production of biologically labile DOM, Miller *et al*. (33) reported the changes in S_{CDOM} measured during photobleaching experiments using long-pass cut-off filters (their table 1). In agreement with our findings, they observed an increase in S_{CDOM} upon solar exposure when using the 425, 380 and 345 nm cut-off wavelength filters and a subsequent decrease in S_{CDOM} as the cut-off wavelength of the filter decreased from 345 to 280 nm. Moreover, for both coastal samples they examined, the S_{CDOM} measured for their lowest cut-off filter treatment (50% T at 280 and 295 nm for the two samples) was smaller than the S_{CDOM} before exposure.

Similar to an earlier work by Osburn *et al*. (36), we have modeled the photobleaching of absorption spectra based on absorbed energy and a spectral weighting function. Although they acknowledged that multiple wavelengths have the ability to bleach absorbance at any given wavelength, Osburn *et al*. modeled photobleaching effect at each wavelength as due to only energy absorbed at that wavelength. However, their model only predicted integrated (average) change in absorption from 290 to 500 nm (PB_{avg}). Here we present a model that does account for wavelength-specific changes in absorbance, and includes the effect of exposure to multiple wavelengths on spectral absorption based on a weighted sum of effects over the full wavelength range of exposure. We modeled spectral variation in the effects of exposure using a "spread function" that qualitatively reproduced the features of the absorption bleaching changes observed with monochromatic exposures (30,32), most importantly that strongest bleaching occurred over a Gaussian-like band with maximum effect near the wavelength of exposure, superimposed on a background of nonspectral bleaching. Thus, the spread function could be specified with just a few parameters, *i.e*. bandwidth, wavelength offset to maximally bleaching irradiance and degree of uniform bleaching. More detailed analyses have shown that the spectral variation of bleaching can depend on the wavelength of irradiance (30,31), nevertheless we were able to model closely the observed changes in absorption with a single spread function. Moreover, the shape of the spread function was similar for all three samples used in the modeling analysis. Estimated FWHM for the Gaussian spread function was between 49 and 92 nm for the different Rhode River samples, consistent with results by Del Vecchio and Blough (30) showing that the FWHM for the region of primary absorption loss was typically about 80 nm for their monochromatic exposure of coastal CDOM samples. Although relatively simple, the model accurately, and consistently, predicted the observed dependence of S_{CDOM} changes on the spectral quality of solar exposure for all samples from the Rhode River system (Figs. 6 and 7).

Spectral absorption and the spread function comprised the most important sources of spectral variation in photobleaching. With these components included, there was little variation in spectral efficiency of photobleaching (relative change in absorption per unit absorbed energy) that could be accounted for using a spectral weighting function. The strongest dependency was in the 101 sample, which had a slight, but significant, positive slope. This equates to a 38% increase in spectral efficiency over the 290–450 range, a relatively small effect. Osburn *et al*. (36) also reported a small positive slope for highly absorbing, humic and strongly photoreactive dissolved material collected from a freshwater *Sphagnum* bog, and slopes that were not significantly different from zero for several other samples. However, other DOM samples did have significantly negative slopes, but the photochemical basis for these differences in the weighting function remains unknown. Weights for photobleaching in the UV-A and UV-B (*i.e*. $W[380]$ and $W[300]$) were consistent with values reported by Osburn *et al*. (36) for CDOM samples with low spectral weighting function slopes.

Colored dissolved organic compounds derived from the tidal marshes and watershed surrounding the Rhode River are highly absorbing and photoreactive, strongly affecting optics and photochemistry, and, thus, also biological activity, in this sub-estuarine ecosystem. Photobleaching of CDOM in both the estuarine and freshwater reaches of this system was strongly dependent on the spectral quality of solar exposure. We showed that a simple predictive model that accounts for wavelength-specific changes and includes the effect of exposure to multiple wavelengths on spectral absorption based on a weighted sum of effects over the full wavelength range of exposure, successfully reproduced the absorption bleaching changes observed in CDOM samples from different sources in the Rhode River. Our results suggest that our simple approach is robust and should be tested for applicability to CDOM from other sources. In addition, it could be applied to the Rhode River system to estimate, or predict, changes in optical properties and carbon fluxes under various atmospheric and in-water conditions.

Acknowledgements—Funds for this work were provided by the Smithsonian Institution Fellowship program and NASA-Goddard Space Flight Center. We thank Jesse Phillips-Kress, James Duls, Sam Benson and Sharyn Hedrick for assistance in the field and laboratory, and Donald Weller for assistance in preparing the map of station locations.

REFERENCES

1. Hedges, J. I. (1992) Global biogeochemical cycles—Progress and problems. *Mar. Chem*. **39**, 67–93.
2. Tranvik, L. J. (1992) Allochthonous dissolved organic-matter as an energy-source for pelagic bacteria and the concept of the microbial loop. *Hydrobiologia* **229**, 107–114.
3. Kieber, D. J. (2000) Photochemical production of biological substrates. In *The Effects of UV Radiation in the Marine Environment* (Edited by S. de Mora, S. Demers and M. Vernet), pp. 130–148. Cambridge University Press, New York.
4. Bricaud, A., A. Morel and L. Prieur (1981) Absorption by dissolved organic matter of the sea (yellow substance) in the UV and visible domains. *Limnol. Oceanogr*. **26**, 43–53.
5. Vodacek, A., N. V. Blough, M. D. DeGrandpre, E. T. Peltzer and R. K. Nelson (1997) Seasonal variation of CDOM and DOC in the Middle Atlantic Bight: Terrestrial inputs and photooxidation. *Limnol. Oceanogr*. **42**, 674–686.
6. Neale, P. J. and D. J. Kieber (2000) Assessing biological and chemical effects of UV in the marine environment: Spectral weighting functions. In *Causes and Environmental Implications of Increased UV-B Radiation* (Edited by R. E. Hester and R. M. Harrison), pp. 61–83. Royal Society of Chemistry, Cambridge, UK.

7. Jordan, T. E., D. L. Correll and D. F. Whigham (1983) Nutrient flux in the Rhode River—Tidal exchange of nutrients by brackish marshes. *Estuar. Coast. Shelf Sci.* **17**, 651–667.
8. Del Castillo, C. E., P. G. Coble, J. M. Morell, J. M. Lopez and J. E. Corredor (1999) Analysis of the optical properties of the Orinoco River plume by absorption and fluorescence spectroscopy. *Mar. Chem.* **66**, 35–51.
9. Chen, R. F., P. Bissett, P. Coble, R. Conmy, G. B. Gardner, M. A. Moran, X. C. Wang, M. L. Wells, P. Whelan and R. G. Zepp (2004) Chromophoric dissolved organic matter (CDOM) source characterization in the Louisiana Bight. *Mar. Chem.* **89**, 257–272.
10. Moran, M. A. and R. E. Hodson (1994) Dissolved humic substances of vascular plant-origin in a coastal marine-environment. *Limnol. Oceanogr.* **39**, 762–771.
11. Opsahl, S. and R. Benner (1997) Distribution and cycling of terrigenous dissolved organic matter in the ocean. *Nature* **386**, 480–482.
12. Moran, M. A. and R. G. Zepp (1997) Role of photoreactions in the formation of biologically labile compounds from dissolved organic matter. *Limnol. Oceanogr.* **42**, 1307–1316.
13. Mopper, K., X. Zhou, R. J. Kieber, D. J. Kieber, R. J. Sikorski and R. D. Jones (1991) Photochemical degradation of dissolved organic carbon and its impact on the oceanic carbon cycle. *Nature* **353**, 60–62.
14. Blough, N. V. and R. G. Zepp (1995) Reactive oxygen species in natural waters. In *Active Oxygen in Chemistry* (Edited by C. S. Foote, J. S. Valentine, A. Greenberg and J. F. Liebman), pp. 280–333. Chapman & Hall, New York.
15. Kieber, R. J., X. L. Zhou and K. Mopper (1990) Formation of carbonyl compounds from UV-induced photodegradation of humic substances in natural waters—Fate of riverine carbon in the sea. *Limnol. Oceanogr.* **35**, 1503–1515.
16. Obernosterer, I., B. Reitner and G. J. Herndl (1999) Contrasting effects of solar radiation on dissolved organic matter and its bioavailability to marine bacterioplankton. *Limnol. Oceanogr.* **44**, 1645–1654.
17. Strome, D. J. and M. C. Miller (1978) Photolytic changes in dissolved humic substances. *Verh. Int. Ver. Limnol.* **20**, 1248–1254.
18. Tranvik, L. J., H. Olofsson and S. Bertilsson (2000) Photochemical effects on bacterial degradation of dissolved organic matter in lake water. In *Microbial Biosystems: New Frontiers, Proceedings of the 8th International Symposium on Microbial Ecology* (Edited by C. R. Bell, M. Brylinski and P. Johnson-Green), pp. 193–200. Atlantic Canada Society for Microbial Ecology, Halifax, Canada.
19. Peterson, B., B. Fry, M. Hullar, S. Saupe and R. Wright (1994) The distribution and stable carbon isotopic composition of dissolved organic carbon in estuaries. *Estuaries* **17**, 111–121.
20. Moran, M. A., W. M. Sheldon and R. G. Zepp (2000) Carbon loss and optical property changes during long-term photochemical and biological degradation of estuarine dissolved organic matter. *Limnol. Oceanogr.* **45**, 1254–1264.
21. Chin, Y. P., G. Aiken and E. Oloughlin (1994) Molecular weight, polydispersity, and spectroscopic properties of aquatic humic substances. *Environ. Sci. Technol.* **28**, 1853–1858.
22. Blough, N. V. and S. A. Green (1995) Spectroscopic characterization and remote sensing of nonliving organic matter. In *Role of Nonliving Organic Matter in the Earth's Carbon Cycle* (Edited by R. G. Zepp and C. Sonntag), pp. 23–45. John Wiley & Sons, New York.
23. Ferrari, G. M. and M. Mingazzini (1995) Synchronous fluorescence spectra of dissolved organic matter (DOM) of algal origin in marine coastal waters. *Mar. Ecol. Prog. Ser.* **125**, 305–315.
24. Belzile, C., J. A. E. Gibson and W. F. Vincent (2002) Colored dissolved organic matter and dissolved organic carbon exclusion from lake ice: Implications for irradiance transmission and carbon cycling. *Limnol. Oceanogr.* **47**, 1283–1293.
25. McKnight, D. M., E. W. Boyer, P. K. Westerhoff, P. T. Doran, T. Kulbe and D. T. Andersen (2001) Spectrofluorometric characterization of dissolved organic matter for indication of precursor organic material and aromaticity. *Limnol. Oceanogr.* **46**, 38–48.
26. Whitehead, R. F., S. de Mora, S. Demers, M. Gosselin, P. Monfort and B. Mostajir (2000) Interactions of ultraviolet-B radiation, mixing, and biological activity on photobleaching of natural chromophoric dissolved organic matter: A mesocosm study. *Limnol. Oceanogr.* **45**, 278–291.
27. Gao, H. Z. and R. G. Zepp (1998) Factors influencing photoreactions of dissolved organic matter in a coastal river of the southeastern United States. *Environ. Sci. Technol.* **32**, 2940–2946.
28. Morris, D. P. and B. R. Hargreaves (1997) The role of photochemical degradation of dissolved organic carbon in regulating the UV transparency of three lakes on the Pocono Plateau. *Limnol. Oceanogr.* **42**, 239–249.
29. Stabenau, E. R., R. G. Zepp, E. Bartels and R. G. Zika (2004) Role of the seagrass *Thalassia testudinum* as a source of chromophoric dissolved organic matter in coastal south Florida. *Mar. Ecol. Prog. Ser.* **282**, 59–72.
30. Del Vecchio, R. and N. V. Blough (2002) Photobleaching of chromophoric dissolved organic matter in natural waters: Kinetics and modeling. *Mar. Chem.* **78**, 231–253.
31. Goldstone, J. V., R. Del Vecchio, N. V. Blough and B. M. Voelker (2004) A multicomponent model of chromophoric dissolved organic matter photobleaching. *Photochem. Photobiol.* **80**, 52–60.
32. Del Vecchio, R. and N. V. Blough (2004) On the origin of the optical properties of humic substances. *Environ. Sci. Technol.* **38**, 3885–3891.
33. Miller, W. L., M. A. Moran, W. M. Sheldon, R. G. Zepp and S. Opsahl (2002) Determination of apparent quantum yield spectra for the formation of biologically labile photoproducts. *Limnol. Oceanogr.* **47**, 343–352.
34. Cullen, J. J. and P. J. Neale (1994) Ultraviolet radiation, ozone depletion, and marine photosynthesis. *Photosynth. Res.* **39**, 303–320.
35. Johannessen, S. C. and W. L. Miller (2001) Quantum yield for the photochemical production of dissolved inorganic carbon in seawater. *Mar. Chem.* **76**, 271–283.
36. Osburn, C. L., H. E. Zagarese, W. Cravero, D. P. Morris and B. R. Hargreaves (2001) Calculation of spectral weighting functions for the solar photobleaching of chromophoric dissolved organic matter in temperate lakes. *Limnol. Oceanogr.* **46**, 1455–1467.
37. Correll, D. L. (1981) Nutrient mass balances for the watershed, headwaters inter-tidal zone, and basin of the Rhode River estuary. *Limnol. Oceanogr.* **26**, 1142–1149.
38. Gallegos, C. L., D. L. Correll and J. W. Pierce (1990) Modeling spectral diffuse attenuation, absorption, and scattering coefficients in a turbid estuary. *Limnol. Oceanogr.* **35**, 1486–1502.
39. Gallegos, C. L., T. E. Jordan, A. H. Hines and D. E. Weller (2005) Temporal variability of optical properties in a shallow, eutrophic estuary: Seasonal and interannual variability. *Estuar. Coast. Shelf Sci.* **64**, 156–170.
40. Jordan, T. E., J. W. Pierce and D. L. Correll (1986) Flux of particulate matter in the tidal marshes and subtidal shallows of the Rhode River estuary. *Estuaries* **9**, 310–319.
41. Correll, D. L. (1977) An overview of the Rhode River watershed program. In *Watershed Research in Eastern North America* (Edited by D. L. Correll), pp. 105–124. Smithsonian Press, Washington, DC.
42. Jordan, T. E. and D. L. Correll (1991) Continuous automated sampling of tidal exchanges of nutrients by brackish marshes. *Estuar. Coast. Shelf Sci.* **32**, 527–545.
43. Lindell, M. J. and H. Rai (1994) Photochemical oxygen consumption in humic waters. *Arch. Hydrobiol. Beih. Ergebn. Limnol.* **43**, 145–155.
44. McKenna, J. H. and P. H. Doering (1995) Measurement of dissolved organic carbon by wet chemical oxidation with persulfate—Influence of chloride concentration and reagent volume. *Mar. Chem.* **48**, 109–114.
45. Lloyd, J. B. F. (1971) Synchronized excitation of fluorescence emission spectra. *Nature-Physical Science* **231**, 64–65.
46. Coble, P. G. (1996) Characterization of marine and terrestrial DOM in seawater using excitation emission matrix spectroscopy. *Mar. Chem.* **51**, 325–346.
47. Neale, P., R. Goodrich and W. Brinley (2005) The Smithsonian-NIST-USDA-FPL Network for Monitoring Solar Ultraviolet Irradiance: Comparison of radiometer measurements and radiative transfer model calculations. In *Service Life Prediction: Challenging the Status Quo* (Edited by J. W. Martin, R. A. Ryntz and

R. A. Dickie), pp. 159–170. Federation of Societies for Coatings Technology, Blue Bell, PA.
48. Vahatalo, A. V. and R. G. Wetzel (2004) Photochemical and microbial decomposition of chromophoric dissolved organic matter during long (months–years) exposures. *Mar. Chem.* **89**, 313–326.
49. Zanardi-Lamardo, E., C. D. Clark, C. A. Moore and R. G. Zika (2002) Comparison of the molecular mass and optical properties of colored dissolved organic material in two rivers and coastal waters by flow field-flow fractionation. *Environ. Sci. Technol* **36**, 2806–2814.
50. Salonen, K. and A. Vahatalo (1994) Photochemical mineralization of dissolved organic matter in Lake Skjervatjern. *Environ. Int.* **20**, 307–312.
51. Lindell, M. J., H. Graneli and S. Bertilsson (2000) Seasonal photoreactivity of dissolved organic matter from lakes with contrasting humic content. *Can. J. Fish. Aquat. Sci.* **57**, 875–885.
52. Vahatalo, A. V., K. Salonen, E. Saski and M. S. Salkinoja-Salonen (2002) Bleaching of color of kraft pulp mill effluents and natural organic matter in lakes. *Can. J. Fish. Aquat. Sci.* **59**, 808–818.